ACTA IMEKO
ISSN: 2221-870X
September 2024, Volume 13, Number 3, 1 - 12

A monitoring platform based on electrical impedance and AI techniques to enhance the resilience of the built environment

Adriano Mancini[1], Gloria Cosoli[2,3], Alessandra Mobili[4], Luca Violini[3], Giuseppe Pandarese[3], Alessandro Galdelli[1], Gagan Narang[1], Elisa Blasi[4], Francesca Tittarelli[4,5], Gian Marco Revel[3]

[1] *Department of Information Engineering, Università Politecnica delle Marche, v. Brecce Bianche 12, 60131 Ancona, Italy*
[2] *Faculty of Engineering, Università Telematica eCampus, v. Isimbardi 10, 22060 Novedrate, Italy*
[3] *Department of Industrial Engineering and Mathematical Sciences, Università Politecnica delle Marche, v. Brecce Bianche 12, 60131 Ancona, Italy*
[4] *Department of Materials, Environmental Sciences and Urban Planning, Università Politecnica delle Marche, v. Brecce Bianche 12, 60131 Ancona, Italy*
[5] *Institute of Atmospheric Sciences and Climate, National Research Council (ISAC-CNR), v. Gobetti 101, 40129 Bologna, Italy*

ABSTRACT
Structural Health Monitoring (SHM) and early warning systems (EWSs) play a pivotal role in enhancing seismic resilience for both buildings and occupants. This paper introduces a monitoring platform that collects electrical impedance data from scaled concrete beams undergoing load and accelerated degradation tests. Artificial Intelligence (AI) algorithms are employed for predictive analysis, scrutinizing historical impedance data, and forecasting future trends. These algorithms adapt to environmental parameters, becoming valuable tools in data-driven decision-making processes. In particular, the study investigates concrete specimens in different test conditions, utilizing a distributed sensor network based on electrical impedance as well as temperature and relative humidity sensors. Real-time data are transmitted to a cloud infrastructure during accelerated degradation tests (both in water and in chloride-rich solution) and in room conditions. An AI-based forecasting approach using Prophet is proposed, ingesting electrical impedance and temperature data, and tested to predict electrical impedance corresponding to approximately 10 % of the time series balancing responsiveness with predictive accuracy, crucial for effective EWS operations and management requirements. The performance of the tested models is evaluated employing metrics such as Mean Average Error (MAE), Root Mean Square Error (RMSE), Mean Absolute Percentage Error (MAPE), and correlation. The proposed approach surpasses statistical methods and deep learning techniques, reporting a MAPE always lower than 3.20 % and a correlation higher than 81.65 % (in wet-dry cycles in water these values are 0.65 Ω and 91.85 %, respectively). This proves to be a promising step towards transparent SHM, which integrates AI models facilitating self-monitoring and early maintenance prediction, thus enhancing the resilience of the built environment.

Section: RESEARCH PAPER

Keywords: monitoring system; seismic protection; Artificial Intelligence; IoT system; sensor network; self-sensing materials

Citation: A. Mancini, G. Cosoli, A. Mobili, L. Violini, G. Pandarese, A. Galdelli, G. Narang, E. Blasi, F. Tittarelli, G. M. Revel, A monitoring platform based on electrical impedance and AI techniques to enhance the resilience of the built environment, Acta IMEKO, vol. 13 (2024) no. 3, pp. 1-12. DOI: 10.21014/actaimeko.v13i3.1722

Section Editor: Francesco Lamonaca, University of Calabria, Italy

Received December 5, 2023; **In final form** May 23, 2024; **Published** September 2024

Funding: This research activity was carried out within the framework of the reCITY project “Resilient City – Everyday Revolution” (reCITY) – PON R&I 2014-2020 e FSC “Avviso per la presentazione di Ricerca Industriale e Sviluppo Sperimentale nelle 12 aree di Specializzazione individuate dal PNR 2015-2020”, identification code ARS01_00592.

Corresponding author: Gloria Cosoli, e-mail: gloria.cosoli@uniecampus.it, g.cosoli@staff.univpm.it

1. INTRODUCTION

Monitoring solutions outperform inspections (both single and periodic ones), since they provide regularly sampled data that can be processed with Artificial Intelligence (AI) algorithms [1] to infer relevant information on the health status of a structure or infrastructure. This capability is instrumental in facilitating effective structural management and decision-making processes, especially in critical scenarios such as emergencies and natural disasters, where the safety and longevity of structures may be compromised. Indeed, continuous monitoring allows us to take interventions as promptly as possible, with a twofold effect: intervention cost optimization and life cycle enhancement [2]. The use of distributed Internet of Things (IoT)-enabled sensors [3] and the predictive capability of AI [4] can be leveraged to develop early warning systems (EWSs), which can make a difference especially when dealing with critical structures and with natural hazards such as earthquakes [5], floods [6], droughts [7], landslides [8], fires [9] and tsunamis [10]. These IoT and AI-based systems not only enable cost-effective monitoring but also contribute significantly to the development of robust strategies for comprehensive risk management [11], with potential applications in diverse settings, including those involving critical infrastructure. Indeed, these systems assist authorities in their decision-making processes and emergency management, with a specific emphasis on prioritizing the preservation of certain buildings [12], [13].

A plethora of sensors can be employed in the field of Structural Health Monitoring (SHM), such as accelerometers [14], strain gages [15], acoustic sensors [16], [17], and electrical impedance sensors [18]. In the last decades, self-sensing materials [19] have been widely employed to enhance both self-sensing and self-monitoring capabilities of construction materials to have a constant and prompt inspection of the structural health of a certain structure or infrastructure [18]. This enhances their resilience against natural hazards, improving the preparedness of the whole community and raising their awareness on the topic.

Distributed sensor networks are particularly suitable, being able to give a comprehensive overview of the structure conditions without the need to progressively move a single sensor to cover a wide area. This paves the way to active monitoring, allowing intervention when needed, promptly maximizing efficiency, and minimizing costs. AI can undoubtedly play a pivotal role in this field, with increasingly growing forecasting capabilities. When considering self-sensing materials and electrical impedance monitoring, for example, AI models can predict electrical impedance (correlated to the structural health status of the material) based on the sequentially gathered data, learning patterns, and trends from historical values. Therefore, if the measured values are far from the foreseen ones, an alert can be generated, and proper actions can be undertaken (e.g., dedicated specific inspections).

A single measurement value is essential to evaluate the current state to plan actions for the future, but the absence of context (history) in a single value represents a limitation. However, extending the current values with N previous measurements allows to set up a sequence of measurements over a certain period and a time series that can be analysed appropriately. Forecasting can build upon historical values, allowing the evaluation of different potential scenarios over different predicting states with diverse forecasting horizons. Predictive algorithms can rely on models based on the underlying physics of the process or could try to map input-output relationships according to data-driven approaches. Therefore, time series forecasting becomes crucial in IoT scenarios with distributed sensor networks where real-time data feed predictive models, which can be used to evaluate if a warning/critical event could happen soon. The forecasting models and EWSs rely on the direct availability of models and data. The choice of the model may vary enormously depending on the application scenario.

Recent advances in AI have enabled machine learning (ML) methods to analyse the fragility of structures during earthquakes. Wen et al. [20] used a convolutional neural network model-based prediction model, StruNet, to develop a rapid prediction model for the vulnerability of reinforced concrete frames based on five dependent variables. The accuracy was tested against four actual cases. Some studies focused on multiple buildings instead of one; for instance, Stojadinović et al. [21] developed a random forest classification model using ML damage classification and representative sampling algorithms. They used this model to develop a vulnerability maintenance cost matrix considering the number of buildings in typical zones. Many studies have demonstrated the potential of ML and deep learning (DL) methods for developing accurate and reliable models to predict the fragility and vulnerability of structures. However, a comparative study that considers the workings of various approaches is needed.

Forecasting models, such as ARIMA, have been proven effective in monitoring-built environments such as bridges and predicting maintenance schedules in advance [22]. Further, a comparative study for the specific application of resilience testing of steel structure bridge data indicated that SARIMAX is a promising model for evaluating time series data and performing anomaly detection simultaneously [23]. Even if these statistical approaches are accurate, they are often complex in implementation and offer little flexibility. ML and DL models can learn complex patterns and relationships from data, making more accurate and reliable forecasts. Recently, newer approaches have emerged across various forecasting applications, such as ML and DL [24], overcoming complex implementation limitations while maintaining comparable or enhanced performance. Facebook Prophet is easy to implement and has showcased promising results in many time series prediction studies [25]. For instance, Prophet has successfully demonstrated good forecasting capabilities for a physical resource like groundwater level [4]. However, its application scenario in built environment resilience monitoring has yet to be tested.

Ensuring accurate data analysis requires a harmonized approach to data ingestion since different applications may utilize the same sensor measurements for various purposes. Therefore, adopting standardized data models presents an opportunity to streamline the integration of applications by providing a common interface (data model) that enhances interoperability. Rapid standardization in the digital market is essential, and the Smart Data Models (SDMs) initiative [26] aims to address the challenge of diverse data models across domains such as smart cities, agri-food, water, energy, logistics, sensors, and smart manufacturing. Data models serve as a fundamental component by defining unified representation formats and semantics for systems and applications to both receive and retrieve data. Various ecosystems have been proposed for this purpose, and in 2018 the European Commission selected the FIWARE ecosystem [27] as a Connecting Europe Facility Building Block. FIWARE is designed to aggregate, manage, and provide access to context information from different sources, describing events in a specified context.

This work aims to present a SHM system based on electrical impedance sensors embedded in self-sensing concretes and the development of AI models with prediction capabilities applied to the absolute value of electrical impedance to be utilized for early warning purposes, relying on the use of Prophet, whose performance is compared to other state-of-the-art approaches. The FIWARE and SDMs initiatives have been considered to simplify the management of the data cycle from the ingestion to the visualization. This signifies a contribution to the current state of SHM-related systems, envisioning its application in a seismic context alongside the potential creation of an EWS.

2. MATERIALS AND METHODS

The experimental study described in this work relies on concrete specimens sensorized with electrical impedance sensors connected to distributed acquisition boards, which in turn were connected to a central hub (Figure 1). Consequently, the data were transmitted to a cloud and handled through an interoperable platform based on the FIWARE initiative. The collected electrical impedance values were processed using various statistical and AI-based models. The details concerning all these aspects are reported in the following subsections.

2.1. Concrete specimens and accelerated degradation tests

Four concrete specimens (10 cm x 10 cm x 50 cm) – labelled as A, B, C, and D – were manufactured according to the mix-design reported in Table 1. The addition of recycled carbon fibers (RCF, Procotex Belgium SA) and biochar (BCH, RES – Reliable Environmental Solutions) provided concretes with self-sensing capability. Portland cement (CEM II/A-LL 42.5R) was used as binder. Three different aggregates were employed, namely a coarse gravel (10-15 mm), a fine gravel (5-10 mm), and a calcareous sand (0-8 mm) as fine aggregate. The water/cement (w/c) ratio was equal to 0.50 by mass. The workability class of the fresh concrete was equal to S5.

Two concrete specimens (i.e., A and B) were preliminarily subjected to load tests (under flexure) until the formation of a crack to evaluate the influence of damages on the penetration of water and 3.5 % NaCl solution, reflecting in changes in terms of electrical impedance. With this regard, accelerated degradation tests were performed by means of weekly wet-dry cycles (2 days wet, and 5 days dry). The details of these tests can be found in works dealing with previous experimental campaigns [28].

2.2. Electrical impedance measurement

Concrete specimens were sensorized with electrode arrays for the measurement of electrical impedance during the casting phase. In particular, the Wenner's method was followed for the sensor configuration and 4 equidistant electrodes were set in a 3-D printed array properly cabled for the connection to the related acquisition board, based on the AD5940 chip (controlled by the embedded unit EVAL-AD5940BIOZ by Analog Devices, USA). The inter-electrode distance was equal to 25 mm; the measurements were performed according to the electrochemical impedance spectroscopy method in a galvanostatic mode with an excitation signal at 10 kHz. This measurement configuration

Table 1. Self-sensing concretes mix-design [kg/m³].

Cement	Water	Air in %	Coarse gravel	Fine gravel	Sand	RCF	BCH
470	235	2.5	476	321	795	1	10

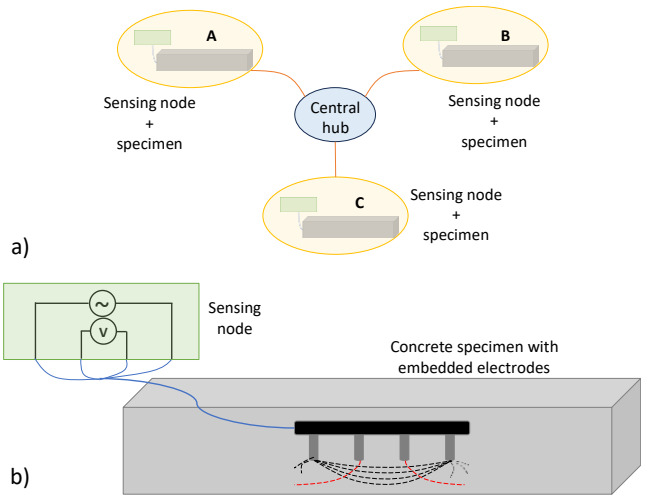

Figure 1. a) Sensor network involving the three concrete specimens and b) sensor node configuration – note that the electrode array is enlarged with respect to real aspect ratio for the sake of readability.

avoids the polarization of both the electrode-material interface and the material itself. In addition, also air temperature and relative humidity were monitored since they directly influence the measured electrical impedance.

Each specimen is sensorized and, together with the related acquisition board, constitutes a sensing node. Hence, each node communicates with a central hub in a star-network architecture (Figure 1). The resulting monitoring system scans all the concrete specimens once per hour and the measurements are planned through a back-end service based on Python. The collected data are then stored both in a local SQLite database and on a cloud.

2.3. AI forecasting models

The acquired input data from the monitoring system (i.e., the time series of electrical impedance and temperature – discarding relative humidity as it is correlated to temperature and this may be redundant) were regularly processed every hour, and, for each specimen under test, the available data were fetched as a time series, which was used to model and re-train several statistical ML, and DL models. More in detail, the analysis employed statistical methods, namely ARIMA, SARIMAX, and a ML technique utilizing Prophet, which is an open-source forecasting procedure. Additionally, the DL method was integrated using NeuralProphet, a hybrid model that merges aspects of Prophet and autoregressive neural networks (AR-Net). Statistical methods rely on specific data assumptions and are interpretable. In contrast, ML and DL models can handle intricate patterns and large-scale data, require comparatively more computational resources, and may lack interpretability. In this case study, a comprehensive evaluation of forecasting abilities was conducted, comparing statistical models with AI techniques (Figure 2). This succinctly aids in comprehending pivotal aspects, such as scalability, interpretability, robustness, and adaptability, offering valuable insights for future studies.

ARIMA is a widely utilized time series forecasting method that combines autoregressive (AR) and moving average (MA) components with differencing to address non-stationary time series data [29]. The model can be represented as a function and sum of three terms, 'p,' 'q,' and 'd', i.e., ARIMA (p, d, q).

The combination of these terms helps in forecasting the future values based on historical data as represented in equations (1) and (2).

$$Y_t = c + \epsilon_t + \sum_{i=1}^{p} \varphi_i X_{t-i} + \sum_{i=1}^{q} \theta_i \epsilon_{t-i} + \delta t \quad (1)$$

$$\mathrm{ARIMA}(p,d,q) = \mathrm{AR}(p) + \mathrm{I}(d) + \mathrm{MA}(q), \quad (2)$$

where:

- p is the autoregressive term; it represents the relationship between an observation and its past at multiple lag values, with higher values indicating a robust autocorrelation at various lags;
- d is the differencing term; it signifies the relationship between the current observation and past value at multiple lag values;
- q is the moving average term; it represents the connection between an observation and a residual error from a moving average model applied to lagged observations;
- θ and φ are coefficients associated with the AR and MA components, respectively;
- ϵ_t is the error term.

The $\mathrm{AR}(p)$ part uses φ_i by multiplying by past observations to represent the autoregressive order defined as 'p'. The MA part uses coefficients θ_i multiplied by past errors ϵ_t − i denotes the moving average order and is represented by 'q'. The part 'd' models the number of past forecast errors that are used for predicting future. These values represent the hyperparameters for the ARIMA model imported from the *statsmodels* library in Python. A higher value of each of these hyperparameters implies a model that relies on more past observations for predicting the current value. Since ARIMA lacks the ability to incorporate seasonal effects, this is expanded by a newer model.

Seasonal ARIMA (SARIMA) with external variables, i.e., SARIMAX, is proposed for subsequent statistical method. The model expands upon ARIMA by incorporating additional seasonal elements and external variables essential for handling periodic patterns in time series data, represented by equation 3:

$$\phi_{\mathrm{p}}(L)\,\phi_{\mathrm{P}}(Ls)\,\Delta^{\mathrm{d}}\Delta_{\mathrm{s}}^{\mathrm{d}} u_{\mathrm{t}} = A(t) + \theta q(L)\,\theta Q(Ls)\zeta_t\,, \quad (3)$$

where it develops on the ARIMA by these terms:

- $\phi_{\mathrm{p}}(L)$ is the autoregressive component of order p;
- $\phi_{\mathrm{P}}(Ls)$ is the seasonal autoregressive component of order p;
- Δ^{d} is the non-seasonal differencing of order d;
- Δ_s^d is the seasonal differencing of order d;
- $A(t)$ represents a deterministic trend, i.e., seasonality;
- $\theta q(L)$ is the seasonal moving average component of order q;
- ζ_t is the seasonal error term;
- s is the seasonal period;
- P is the seasonal autoregressive component of order P;
- D is the seasonal differencing of order D;
- Q is the seasonal moving average component of order Q.

SARIMAX integrates seasonal autoregressive (P), seasonal differencing (D), and seasonal moving average (Q) terms alongside the non-seasonal ARIMA components (p, d, q). The seasonal autoregressive term (P) captures the relationship between an observation and its seasonal lag values, accounting for the seasonal patterns within the data. Similarly, the seasonal moving average (Q) term establishes the relationship between an observation and the residual error from a seasonal moving average model applied to seasonal lagged observations. Seasonal differencing 'D' is applied to the seasonal observations, ensuring the data seasonal stationarity. SARIMAX comprehensively addresses both non-seasonal and seasonal patterns in time series data by incorporating these seasonal components and non-seasonal ARIMA elements.

Building on the statistical approaches, two advanced forecasting in the realm of AI realized through ML and DL approaches were used. The first approach is Prophet, which represents the time series as the sum of three components: (i) trend, (ii) seasonality, and (iii) holidays, as shown in equation 4:

$$y(t) = g(t) + s(t) + h(t) + \varepsilon(t)\,, \quad (4)$$

where:

- $g(t)$ is trend function, modelling non-periodic changes; it can be logarithmic;
- $s(t)$ is the seasonality function, relying on the Fourier series, providing a flexible model of periodic effects to model changes that are repeated at regular time intervals (e.g., weekly and yearly seasonality); it is also possible to have more than one seasonality in the same series;
- $h(t)$ represents holidays; it models irregular events that temporarily alter the time series;
- $\varepsilon(t)$ is the error term, representing changes in the time series that the model does not capture; it is regarded as a normal distribution.

Prophet works by decomposing the entered time series into additive components modelling the trends as piecewise linear logistic growth curve. Seasonality is captured through Fourier series expansion. It can model abrupt patterns, which can be entered on a custom basis through holiday effects which are, however, not activated in this case study.

NeuralProphet is a natural extension to Prophet and is a fully connected neural network based on the modular composability of different components according to equation 5:

$$\widetilde{y_t} = T(t) + S(t) + E(t) + F(t) + A(t) + L(t)\,, \quad (5)$$

Where:

- $\widetilde{y_t}$ is the predicted value;
- $T(t)$ is the trend at time t;
- $S(t)$ is the Seasonal effects at time t;
- $E(t)$ is an event and holiday effects at time t;
- $F(t)$ is the regression effects at time t for future-known exogenous variables;
- $A(t)$ is the auto-regression effects at time t based on past observations;
- $L(t)$ is the regression effects at time t for lagged observations of exogenous variables.

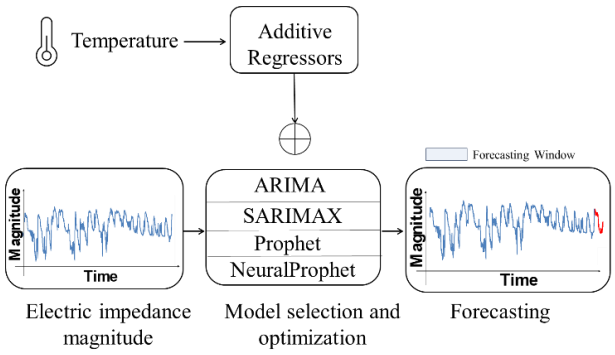

Figure 2. Graphical representation of time-series forecasting from ancillary rious models.

NeuralProphet adds features such as automatic selection of hyperparameters during training and the ability to add an auto-regressive component managed by the AR-Net neural network model. Further hidden layers and/or more output nodes can be added in the case of multi-step forecasting.

2.4. Data ingestion and forecasting

Data ingestion and processing are essential for forecasting electrical impedance using statistical or AI-based algorithms. This was realized through a cloud architecture devised specifically for ingesting data acquired by the sensor network outlined in Section 2.1. The architecture adopts a serverless approach, utilizing a NoSQL key-value database for storage, with DynamoDB from Amazon Web Services (AWS). Data were ingested through a dedicated lambda function triggered by the API gateway, which receives HTTPS requests from a local client installed on the machine connecting all the sensor nodes. The execution of the lambda function was scheduled at regular intervals (every hour), aiding in forecasting. The hourly interval struck a balance between capturing detailed time series data and maintaining manageable data volumes, allowing us to update and re-train our ML and DL models efficiently. Should the predicted values exceed a predetermined threshold, a trigger signal is dispatched to a dedicated event bus to notify subscribed applications. Simultaneously, an alternative architecture was employed for data storage within the FIWARE ecosystem (https://www.fiware.org). A custom smart data model was crafted to accommodate the electrical impedance signals obtained from the sensor network (Section 2.1). The FIWARE ecosystem leverages QuantumLeap (quantumleap.readthedocs.io) and CrateDB (crate.io/) for time-series storage, ensuring easier data retrieval and manipulation procedures.

The models were trained using a combination strategy of model selection and tuning based on cross-validation through training data measuring predictive errors on validation data, as showcased in Figure 3. The input data to the model included the absolute value of electrical impedance (|Z|) and temperature, which was utilized as an additive regressor (relative humidity was not employed, being correlated to temperature). This minimalist approach not only simplifies the modelling process, but also aligns with the principles of effective early warning systems, which benefit from streamlined and efficient data utilization to provide timely and reliable alerts. The additive regressor indirectly aids in the learning process during its training process,

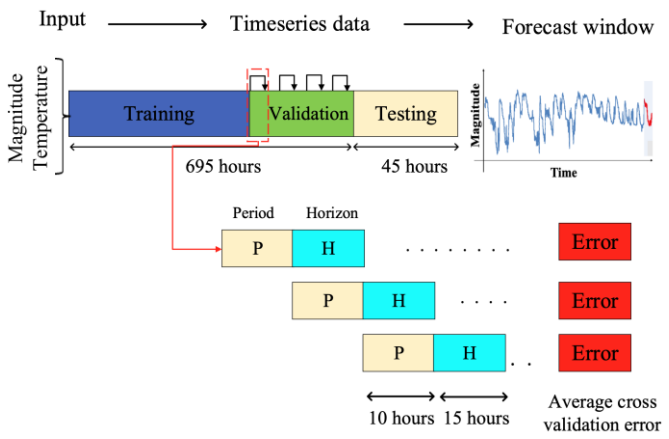

Figure 3. Rolling cross-validation strategy applied to electrical impedance time series data to obtain forecast window.

where the model additionally learns from temperature information and adjusts forecast accuracy. This choice was informed by the strong daily seasonality observed in the data, attributed to temperature gradients between day and night. The input data were normalized using a MinMax scaler to ensure uniformity in scale in the target variable and across features and facilitated convergence of the model during learning process. The data were subsequently fed into the model, which underwent training on the designated training dataset, employing cross-validation to fine-tune hyperparameters, ultimately utilized for making accurate and optimized forecasts. Cross-validation evaluates how well the model generalizes to new data and assesses its performance by splitting the training dataset into multiple training and testing subsets.

The determination of the multiple splits of the training data, which were used for cross-validation, was guided by key parameters: period and horizon. The period parameter specifies the length of a seasonal cycle, and the horizon parameter defines the duration for which future predictions are made. During each cross-validation fold, the model was trained on a predefined initial training set and iterated by expanding the training size in every period, thus making predictions for the length of the horizon. The process iterated across the entire time series, providing a robust assessment of the model performance across different data segments. Following the forecasting process, the results were denormalized, restoring the data to their original scale for meaningful interpretation and application.

2.5. Training settings and hyperparameter tuning

The most suitable hyperparameters were used to make a final prediction on unseen testing data, and error metrics were calculated and used for comparison with other approaches. This rigorous methodology ensured that the selected model performed well during training and demonstrated superior forecasting capabilities on unseen data, providing a reliable and effective solution for forecasting needs. Various forecasting accuracy empirics were computed to validate and compare the proposed approach to the other state-of-the-art approaches. The same tuning procedure was also performed for ARIMA, SARIMAX, and NeuralProphet to conduct a fair comparison test. The validation dataset used cross-validation with 10 hours period and 15 hours horizon. Conversely, for the Prophet model, the developers provided special functions for optimizing hyperparameters with cross-validation; for the ARIMA and SARIMAX models, ad-hoc development was necessary.

The testing of various concrete specimens was conducted at different time intervals under three different conditions: (i) wet-dry cycles with water, (ii) wet-dry cycles with 3.5 % NaCl solution, and (iii) room conditions. Table 2 illustrates the time intervals considered for each test.

The forecast in terms of |Z| was performed over 45 intervals (~10 % of time series), corresponding to 45 hours (i.e., approximately two days). The forecasting performance was evaluated through the following metrics:

Table 2. Table of period settings for each specimen.

Setting test	Start Period	End Period
Wet-dry cycles with water	30-05-2023	27-06-2023
Wet-dry cycles with 3.5 % NaCl solution	28-06-2023	26-07-2023
Room conditions	03-08-2023	31-08-2023

- Mean Absolute Error (MAE), which is the absolute value of the difference between paired accurate and predicted data;
- Mean Absolute Percentage Error (MAPE), which is the percentage expression of MAE obtained through the normalization by the real data;
- Root Mean Square Error (RMSE), which is the average difference between predicted and real data;
- Correlation, which is the strength and direction of the linear relationship between predicted and actual values.

3. RESULTS

The comprehensive data compiled in Table 3 encapsulates the results from various tests conducted on all specimens across multiple scenarios and selected empirics. The visual comparison of the results is presented in Figure 4, Figure 5, Figure 6, and Figure 7. The study categorizes concrete specimens into two types: those with cracks (i.e., A and B) and the undamaged specimens (i.e., C and D). The distinction in the performance of the models is particularly noteworthy in these different scenarios, which positions the proposed approach as a valuable tool, potentially finding application in EWSs for the evaluation of concrete health status. Notably, the model based on Prophet offers superior performance with lower error metrics and higher correlations in tested samples with and without cracks. For instance, in the case of the specimen A (cracked) the proposed model performs better in all the tested conditions. Considering wet-dry cycles in water, the model obtains MAPE of 0.60 % versus 0.80 %, 3.60 %, and 1.40 % obtained by other models, namely ARIMA, SARIMAX, and NeuralProphet. The same specimen in 3.5 % NaCl solution produced MAPE values of 3.16 % compared to 8.16 %, 8.90 %, and 8.20 % obtained with the above-mentioned other models. Additionally, the correlation with actual data is also higher, namely 95.73 %, in contrast to 90.12 %, 88.68 %, and 25.76 % for the specimen exposed to wet-dry cycles in water. Considering the same specimen in wet-dry cycles in 3.5 % NaCl solution, the values are equal to 90.86 %, -61.13 %, -58.37 %, and -30.59 %, which signifies an opposite trend compared to the original values.

For the specimen B, in the case of wet-dry cycles in water, the proposed model consistently outperforms other state-of-the-art models, showcasing a MAPE of 2.0 %, which is notably lower than the values of 2.30 %, 5.37 %, and 7.57 % obtained by ARIMA, SARIMAX, and NeuralProphet, respectively. The correlation with actual data is considerably higher for the proposed model, reaching 72.66 %. This is lower than the best value obtained with ARIMA with 91.85 %; however, it is possible to visually notice that ARIMA considerably fails to capture the trends in the data, given that it just passes through the observed data as a straight line, obtaining a higher correlation. The correlation value for the proposed model is better than the other models (NeuralProphet achieves -12.58 % and SARIMAX 57.70 %, respectively). This trend is also followed during room conditions, where ARIMA performs slightly better in terms of errors, with a MAPE of 0.2 % in comparison to the proposed model with 0.6 %. However, the proposed model captures the intricate patterns and has lower errors compared to all the other models, i.e., 1.13 % and 1.25 % for SARIMAX and NeuralProphet, respectively. The proposed model has a much higher correlation than all other models, with 81.66 % compared to 78.23 %, 73.23 %, and 16.39 % for ARIMA, SARIMAX, and NeuralProphet, respectively. For the same specimen during wet-dry cycles in 3.5 % NaCl solution, the proposed model excels with a MAPE of 7.30 %, outshining ARIMA, SARIMAX, and NeuralProphet, which report MAPE values of 20.48 %, 22.45 %, and 18.99 %, respectively. The correlation with actual data for the proposed model stands at 90.40 %, demonstrating superior performance compared to values of -67.69 %, 86.66 %, and -14.31 % for the other models.

Additionally, for the undamaged specimens, in the case of the specimen C, the proposed model demonstrates superior forecasting performance across different environmental conditions. In the instance of wet-dry cycles in water, it achieves an impressive MAPE of 1.12 %, outshining other prominent models such as ARIMA, SARIMAX, and NeuralProphet, which report MAPE values of 2.30 %, 1.24 %, and 3.12 %, respectively. Furthermore, the correlation with actual data is notably higher for the proposed model, standing at 76.65 %, compared to values ranging from 19.32 % to 36.08 % for the other models. Similarly, during wet-dry cycles in 3.5 % NaCl solution, the proposed model excels with a MAPE of 1.62 %, surpassing ARIMA, SARIMAX, and NeuralProphet, which report MAPE values of 4.32 %, 3.19 %, 2.73 %, respectively.

The correlation with actual data for the model is robust at 86.66 %, demonstrating superior performance compared to values ranging from -65.38 % to 73.33 % for the other models.

Table 3. Standard evaluation metric for comparisons between the proposed approach and other state-of-the-art architectures.

		Cracked								**Intact (undamaged)**							
Specimen		A				B				C				D			
Test condition	Approach	MAE (Ω)	RMSE (Ω)	MAPE (%)	Correlation (%)	MAE (Ω)	RMSE (Ω)	MAPE (%)	Correlation (%)	MAE (Ω)	RMSE (Ω)	MAPE (%)	Correlation (%)	MAE (Ω)	RMSE (Ω)	MAPE (%)	Correlation (%)
Wet-dry cycles in water	ARIMA	2.27	2.88	0.86	90.12	10.83	13.30	2.30	**91.85**	5.86	6.36	2.30	32.13	3.97	4.49	1.94	10.43
	SARIMA	9.73	11.61	3.65	88.68	25.21	28.02	5.37	-12.58	**2.87**	**3.51**	**1.12**	36.08	2.90	3.51	1.42	-4.61
	Prophet	**1.71**	**2.03**	**0.65**	**95.73**	**9.47**	**11.60**	**2.02**	72.66	3.14	3.83	1.24	**76.65**	**1.43**	**1.66**	**0.70**	**65.09**
	NeuralProphet	3.70	4.54	1.40	25.76	35.36	36.90	7.57	57.70	7.93	8.67	3.12	19.32	2.89	3.58	1.42	22.30
Wet-dry cycles in 3.5 % NaCl solution	ARIMA	18.79	33.13	9.52	-61.13	57.51	98.44	20.48	-67.69	12.20	13.74	4.32	4.25	8.49	9.39	3.90	85.67
	SARIMA	17.68	31.66	8.99	-58.37	63.95	**5.72**	22.45	86.66	9.07	11.34	3.19	-65.38	6.23	7.71	2.84	33.69
	Prophet	**7.30**	**9.28**	**3.16**	**90.86**	**25.41**	31.71	**7.30**	**90.40**	**4.59**	**5.72**	**1.62**	**86.66**	**2.59**	**2.94**	**1.19**	**88.00**
	NeuralProphet	16.29	27.70	8.20	-30.59	54.98	86.42	18.99	-14.31	7.72	9.13	2.73	73.33	6.20	7.15	2.84	73.85
Room conditions	ARIMA	10.96	13.90	2.88	67.64	**1.69**	**2.08**	**0.29**	78.23	4.73	5.84	1.18	76.72	7.54	9.17	2.53	71.00
	SARIMA	10.70	13.58	2.81	68.01	6.61	7.96	1.13	73.23	8.67	10.33	2.16	-26.72	9.20	10.99	3.09	71.92
	Prophet	**2.50**	**2.87**	**0.66**	**93.63**	3.49	3.81	0.60	**81.66**	**2.03**	**2.39**	**0.51**	**88.53**	**2.13**	**2.41**	**0.71**	**92.92**
	NeuralProphet	34.92	42.11	9.21	26.69	73.47	86.62	12.57	16.39	37.19	37.70	9.32	9.77	24.91	25.24	8.37	10.11

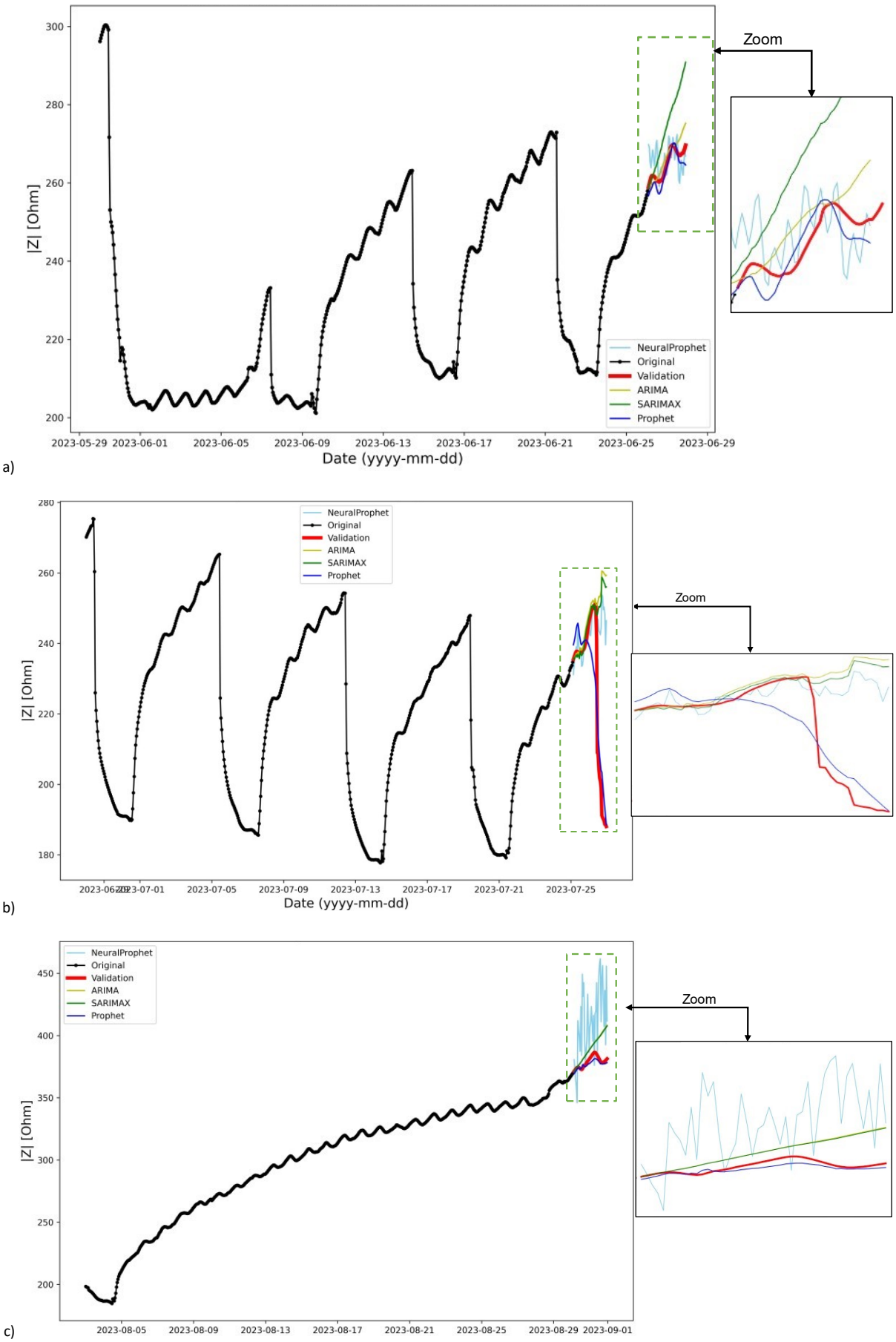

Figure 4. Forecasting using different approaches for a Specimen A (cracked) during a) wet-dry cycles in water, b) wet-dry cycles in 3.5 % NaCl solution, and c) room conditions.

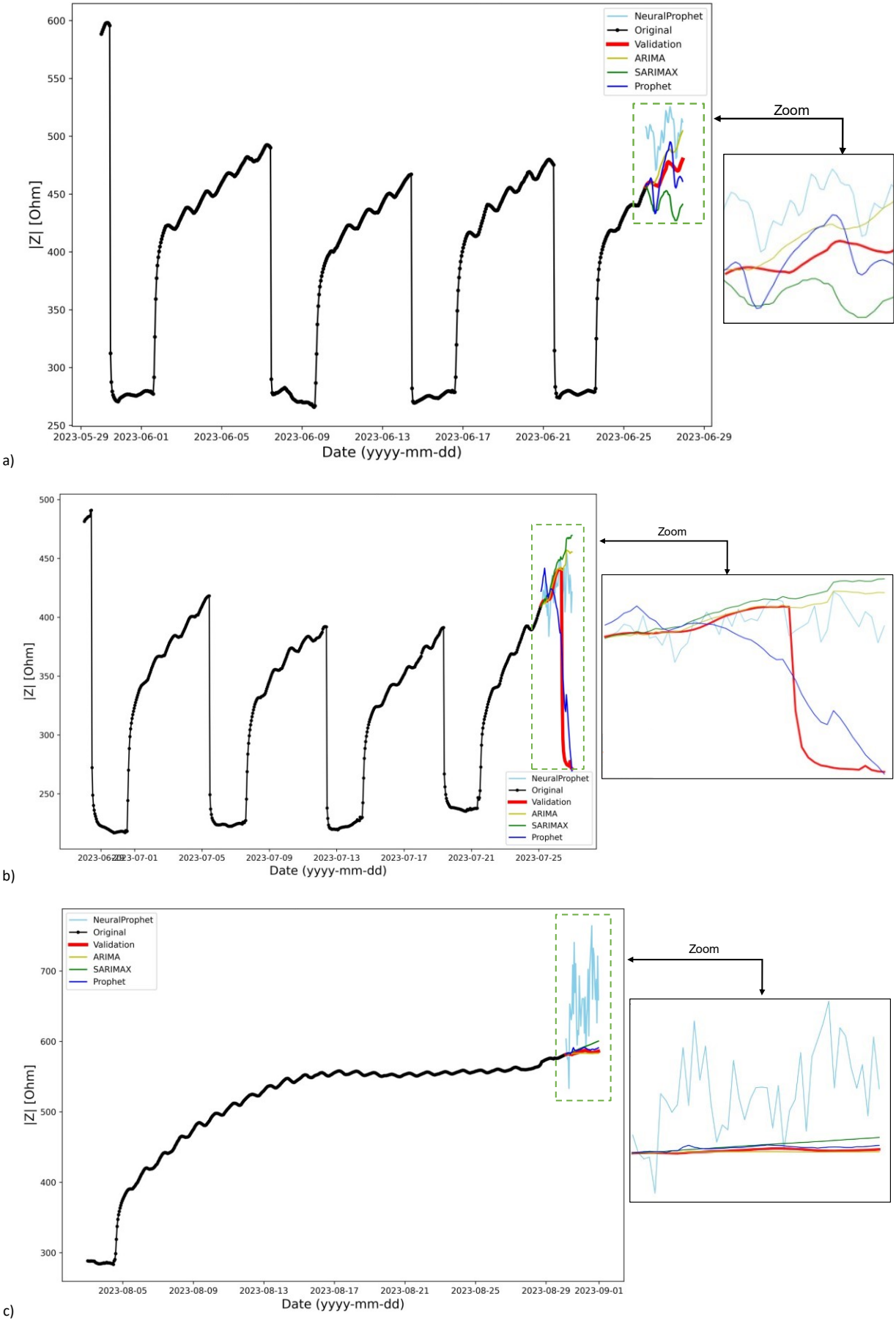

Figure 5. Forecasting using different approaches for specimen B (cracked) during a) wet-dry cycles in water, b) wet-dry cycles in 3.5 % NaCl solution c) room conditions.

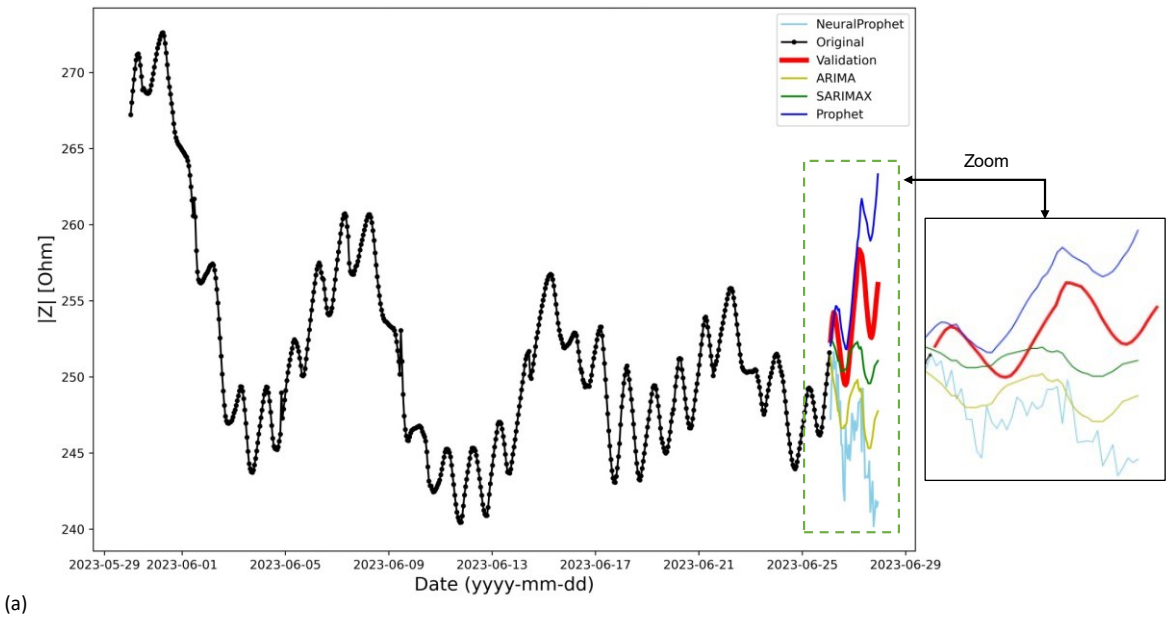

(a)

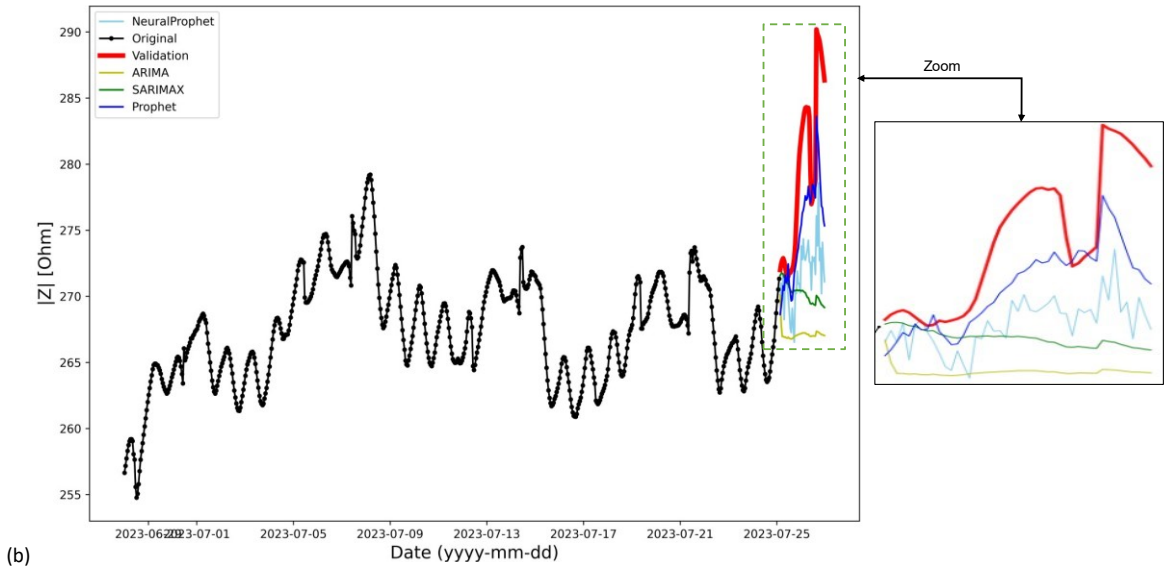

(b)

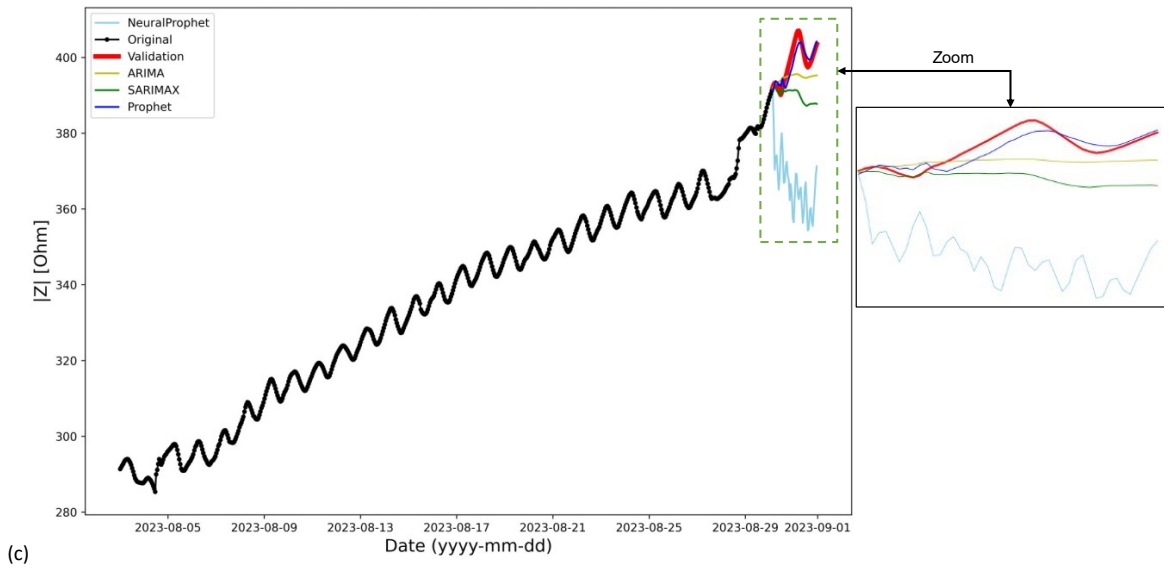

(c)

Figure 6. Forecasting using different approaches for specimen C (undamaged) during a) wet-dry cycles in water, b) wet-dry cycles in 3.5 % NaCl solution, and c) room conditions.

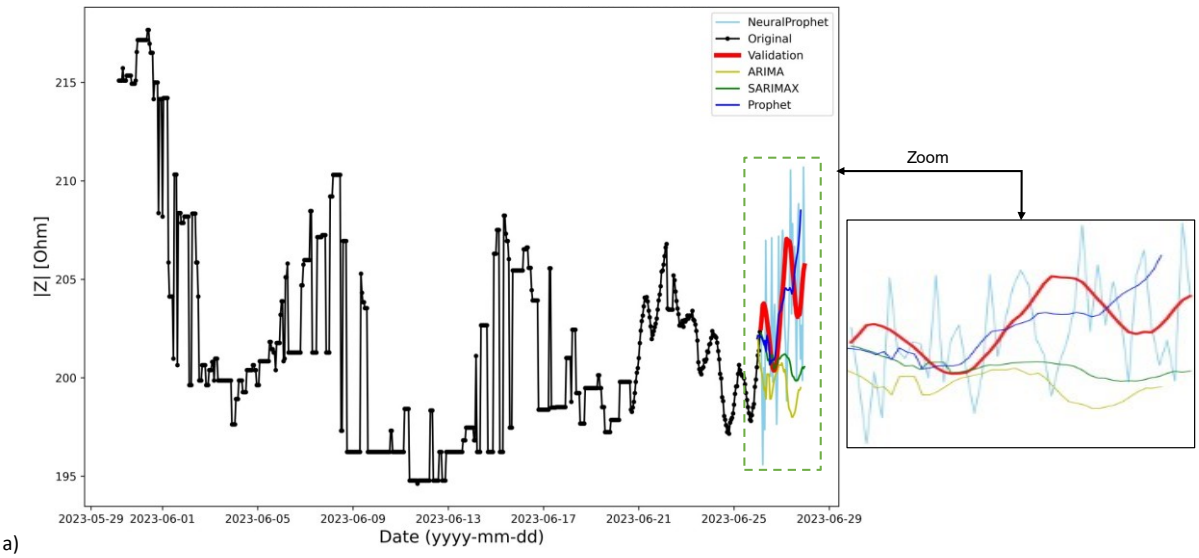

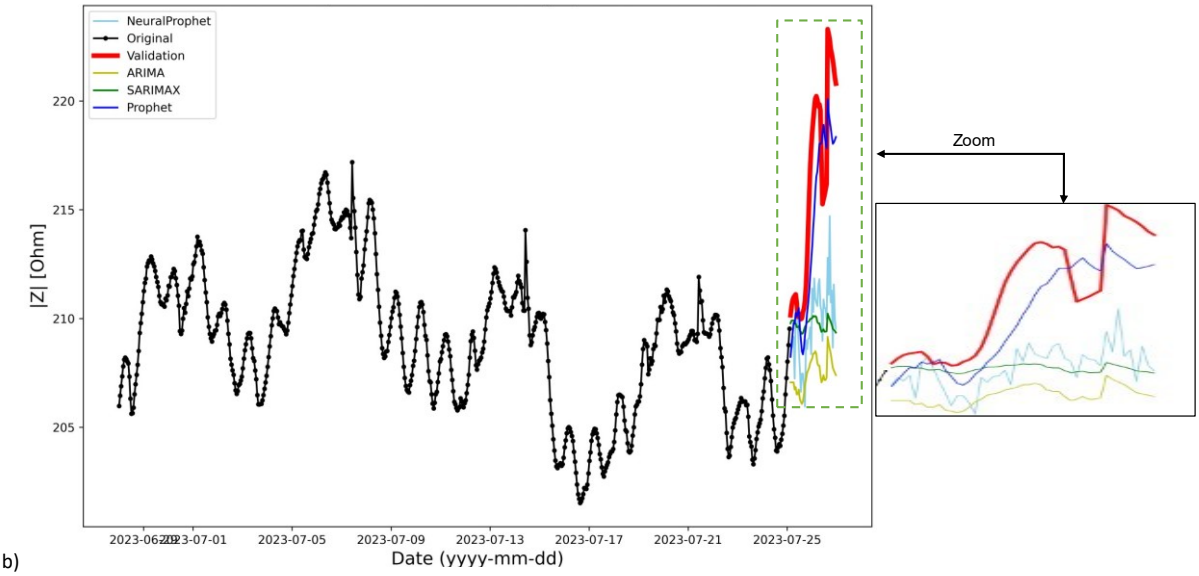

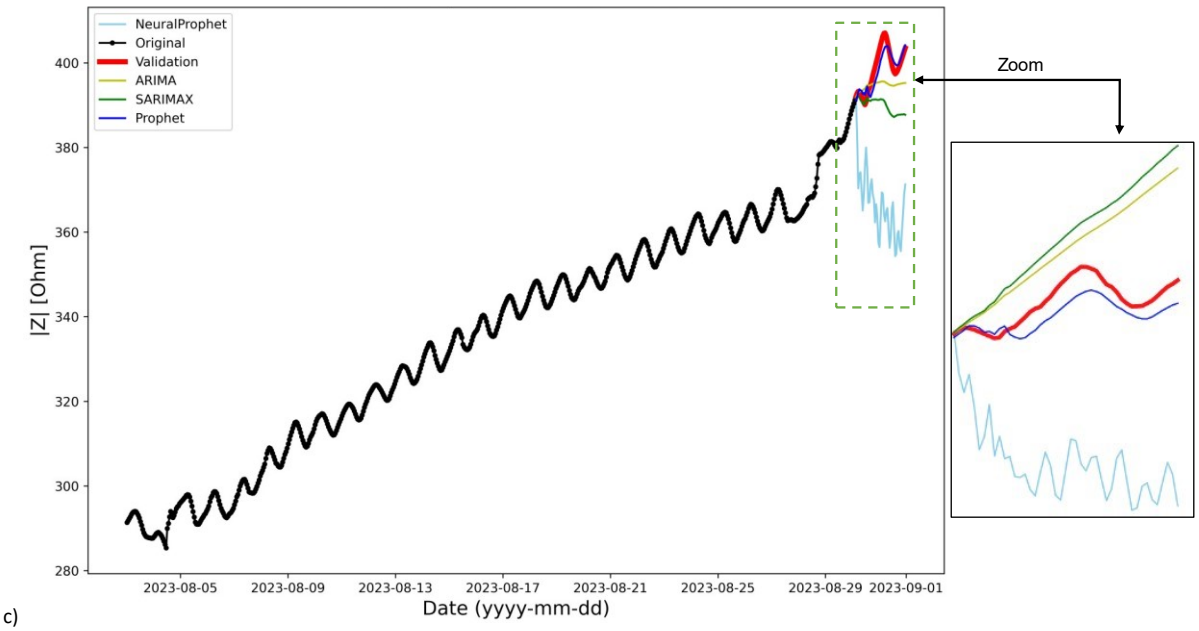

Figure 7. Forecasting using different approaches for specimen D (undamaged) during a) wet-dry cycles in water, b) wet-dry cycles in 3.5 % NaCl solution, and c) room conditions.

In room conditions, the specimen C continues to exhibit the effectiveness of the proposed approach with a MAPE of 0.51 %, outperforming ARIMA, SARIMAX, and NeuralProphet, which record MAPE values of 1.18 %, 2.16 % and 9.32 %, respectively. The correlation with actual data is notably high, standing at 88.53 %, in comparison to values equal to 76.72 %, -26.72 %, and 9.77 % for the other models. The proposed model in case of the specimen D during wet-dry cycles in water obtains MAPE of 0.70 % versus 1.90 %, 1.42 %, and 1.42 % obtained by other state-of-the-art models (i.e., ARIMA, SARIMAX, and NeuralProphet, respectively). The same specimen in wet-dry cycles in 3.5 % NaCl solution produces MAPE values of 1.19 % compared to 3.90 %, 2.80 %, and 2.80 %. The correlation with actual data is also higher and for the proposed model is 65.09 % in contrast to 10.43 %, -4.6 %, and 22.30 % for the case of specimen exposed to wet-dry cycles in water. For the same specimen in 3.5 % NaCl solution the values are equal to 88.00 %, 85.67 %, 33.69 % and 73.85 %. In room conditions, it is observed that ARIMA performs slightly better in terms of MAPE, MAE, and RMSE. However, the proposed model has a strong correlation of 81.66 % compared to 78.23 %, signifying that it has correctly captured seasonal patterns in the data. The consistent results underscore the robust and reliable forecasting capabilities of the proposed Prophet-based model across different scenarios for all the specimens.

4. DISCUSSION AND CONCLUSIONS

The present work reports the results from the monitoring of concrete specimens with self-sensing capabilities through a sensor network based on electrical impedance measurements, performed according to the Wenner's method to maximize the signal quality. Self-sensing concretes were monitored since May 2023 to August 2023; the time-series data were ingested by a cloud architecture through a dedicated lambda function. Statistical and advanced artificial intelligence-based approaches to forecast electrical impedance (in particular, its absolute value) were used and quantitative results were discussed. The empirical findings highlight the informative potential of AI-based algorithms in assessing the condition of cement-based elements subjected to accelerated degradation tests. In this context, the selection of a stationary 45-hour forecast window (approximately 10 % of the time series) was determined to provide a viable trade-off between timely responsiveness and computational feasibility, aiming to optimize the utility of forecasts in the operational settings of the EWSs. Notably, the proposed approach, based on Prophet, emerges as a promising solution for forecasting abilities needed in EWSs to enhance the resilience of the built environment. The results underscore its ability to accurately predict the absolute value of electrical impedance, exhibiting lower error ranges and heightened correlation across diverse specimens exposed to different conditions (namely wet-dry cycles in water and 3.5 % NaCl solution as well as room conditions).

The model demonstrates the capability of the system to predict the trend of absolute electrical impedance value for concrete specimens in different conditions in comparison with other state-of-the-art models. Further, the model conveniently utilizes temperature information, improving its accuracy. The proposed approach offers better performance than DL (based on NeuralProphet) or statistical approaches (i.e., ARIMA and SARIMAX), considering the performance metrics. When visualized for other approaches, the predictions either have higher fluctuations (NeuralProphet) or miss out on seasonal patterns (ARIMA and SARIMAX). This substantiates the Prophet-based model efficacy and robustness in capturing intricate patterns, affirming its suitability for concrete monitoring applications. The forecasted values not only serve as a tool for understanding near-future trends but also play a crucial role in issuing timely warnings to users in case the absolute values exceed the set thresholds within the model. The warning is raised if the ancillary data (consolidated) and forecasted ones that belong to a time window of n samples have a median that overtakes the threshold. Importantly, the proposed system allows a promising solution for maintenance planning and risk management, enabling facility managers to optimize intervention schedules and resources effectively, thus reflecting on the economic and safety aspects of SHM [30].

The modularity of the selected model proves pivotal in this context, allowing for the consideration of various components, from seasonality to complex trends. This adaptability enables customization to specific application contexts, such as seismic considerations, ensuring optimal accuracy for the target application. Leveraging digital tools, this model can contribute significantly to the optimization of both the quality and life cycle of living environments, thanks to the possibility of being integrated into monitoring systems, also with the possibility of being sided by different types of sensors (e.g., sensors for acoustic emissions [31], Global Navigation Satellite System and accelerometers [32]), hence exploiting data-fusion techniques [33]. In the future, it is proposed to extend the performed analysis by comparing the proposed forecasting approach, based on the Prophet model, with emerging methods such as transformer-based sequence-to-sequence (Seq2seq) models. Transformers based forecasting approaches, particularly in seq2seq tasks, offer advanced capabilities such as attention mechanisms, adaptability to diverse data patterns, and enhanced performance in some applications. The data in SHM application have showcased sequential patterns that have strong sequences of seasonal dependence on daily temperature and conditions such as presence of water or salts. Further, considerations for varying forecast windows can provide insights into the scalability and flexibility of the model under different operational conditions. The adaptability of the model to different scenarios ensures its effectiveness across varying operational demands. Therefore, extending the analysis by including a transformer-based model along with a varying forecast horizon will be an interesting future development.

ACKNOWLEDGEMENT

This research activity was carried out within the framework of the reCITY project "Resilient City – Everyday Revolution" (reCITY) – PON R&I 2014-2020 e FSC "Avviso per la presentazione di Ricerca Industriale e Sviluppo Sperimentale nelle 12 aree di Specializzazione individuate dal PNR 2015-2020", identification code ARS01_00592.

REFERENCES

[1] R. Zinno, S. S. Haghshenas, G. Guido, A. Vitale, Artificial Intelligence and Structural Health Monitoring of Bridges: A Review of the State-of-the-Art, IEEE Access, vol. 10, 2022, pp. 88058–88078.
DOI: 10.1109/access.2022.3199443

[2] W. R. de Sitter, Costs of service life optimization 'The Law of Fives.' Comité Euro-International du Béton, 1984, pp. 131–134.

[3] F. Lamonaca, C. Scuro, P. F. Sciammarella, R. S. Olivito, D. Grimaldi, D. L. Carnì, A layered IoT-based architecture for a distributed structural health monitoring system system, Acta IMEKO, vol. 8, no. 2, June 2019, pp. 45–52. DOI: 10.21014/acta_imeko.v8i2.640

[4] A. Galdelli, G. Narang, L. Migliorelli, A. D. Izzo, A. Mancini, P. Zingaretti, An AI-Driven Prototype for Groundwater Level Prediction: Exploring the Gorgovivo Spring Case Study, Lect. Notes Comput. Sci. (including Subser. Lect. Notes Artif. Intell. Lect. Notes Bioinformatics), vol. 14234 LNCS, 2023, pp. 418–429. DOI: 10.1007/978-3-031-43153-1_35

[5] G. Cremen, C. Galasso, Earthquake early warning: Recent advances and perspectives, Earth-Science Rev., vol. 205, June 2020, p. 103184. DOI: 10.1016/J.EARSCIREV.2020.103184

[6] W. Haszerila Wan Hasan, A. Z. Jidin, S. A. Che Aziz, N. Rahim, Flood disaster indicator of water level monitoring system, Int. J. Electr. Comput. Eng., vol. 9, no. 3, 2019, pp. 1694–1699. DOI: 10.11591/ijece.v9i3.pp1694-1699

[7] L. Sharafi, K. Zarafshani, M. Keshavarz, H. Azadi, S. Van Passel, Drought risk assessment: Towards drought early warning system and sustainable environment in western Iran, Ecol. Indic., vol. 114, Jul. 2020, p. 106276. DOI: 10.1016/J.ECOLIND.2020.106276

[8] F. Guzzetti, S. L. Gariano, S. Peruccacci, M. T. Brunetti, I. Marchesini, M. Rossi, M. Melillo, Geographical landslide early warning systems, Earth-Science Rev., vol. 200, Jan. 2020, p. 102973. DOI: 10.1016/J.EARSCIREV.2019.102973

[9] M. Findlay, D. Peaslee, J. R. Stetter, S. Waller, A. Smallridge, Distributed Sensors for Wildfire Early Warnings, J. Electrochem. Soc., vol. 169, no. 2, Feb. 2022, p. 020553. DOI: 10.1149/1945-7111/AC5344

[10] T. Srinivasa Kumar, S. Manneela, A Review of the Progress, Challenges and Future Trends in Tsunami Early Warning Systems, J. Geol. Soc. India, vol. 97, no. 12, Dec. 2021, pp. 1533–1544. DOI: 10.1007/S12594-021-1910-0/METRICS

[11] A. Galdelli, A. Mancini, E. Frontoni, A. N. Tassetti, A feature encoding approach and a cloud computing architecture to map fishing activities, Proc. ASME Des. Eng. Tech. Conf., vol. 7, 2021. DOI: 10.1115/DETC2021-69799

[12] M. P. Limongelli, Monitoraggio strutturale per la protezione sismica del patrimonio edilizio, Tra Prev. e cura la Prot. del Patrim. Edil. dal rischio Sism., pp. 36–48, 2013. [in Italian]

[13] R. Ceravolo, G. de Lucia, E. Lenticchia, G. Miraglia, Seismic structural health monitoring of cultural heritage structures, Springer Tracts Civ. Eng., pp. 51–85, 2019. DOI: 10.1007/978-3-030-13976-6_3/COVER

[14] G. De Alteriis, E. Caputo, R. S. Lo Moriello, On the suitability of redundant accelerometers for the implementation of smart oscillation monitoring system: Preliminary assessment, Acta IMEKO, vol. 12, no. 2, May 2023, pp. 1–9. DOI: 10.21014/ACTAIMEKO.V12I2.1532

[15] C. Scuro, D. L. Carnì, F. Lamonaca, R. S. Olivito, G. Milani, Preliminary study of an ancient earthquake-proof construction technique monitoring via an innovative structural health monitoring system, Acta IMEKO, vol. 10, no. 1, 2022, pp. 47–56. DOI: 10.21014/ACTA_IMEKO.V10I1.819

[16] J. O. Willberry, M. Papaelias, Structural Health Monitoring Using Fibre Optic Acoustic Emission Sensors, Sensors 2020, vol. 20, no. 21, Nov. 2020, p. 6369. DOI: 10.3390/S20216369

[17] F. Lamonaca, A. Carrozzini, D. Grimaldi, R. S. Olivito, Improved monitoring of acoustic emissions in concrete structures by multi-triggering and adaptive acquisition time interval, Measurement. 59 (2015), pp. 227–236. DOI: 10.1016/J.MEASUREMENT.2014.09.053

[18] N. Giulietti, P. Chiariotti, G. Cosoli (+ another 6 authors), Continuous monitoring of the health status of cement-based structures: electrical impedance measurements and remote monitoring solutions, Acta IMEKO, vol. 10, no. 4, Dec. 2021, pp. 132–139. DOI: 10.21014/ACTA_IMEKO.V10I4.1140

[19] W. Li, F. Qu, W. Dong, G. Mishra, S. P. Shah, A comprehensive review on self-sensing graphene/cementitious composites: A pathway toward next-generation smart concrete, Constr. Build. Mater., vol. 331, May 2022, p. 127284. DOI: 10.1016/J.CONBUILDMAT.2022.127284

[20] W. Wen, C. Zhang, and C. Zhai, "Rapid seismic response prediction of RC frames based on deep learning and limited building information," Eng. Struct., vol. 267, Sep. 2022, p. 114638. DOI: 10.1016/J.ENGSTRUCT.2022.114638

[21] Z. Stojadinović, M. Kovačević, D. Marinković, B. Stojadinović, Rapid earthquake loss assessment based on machine learning and representative sampling, Earthq. Spectra, vol. 38, no. 1, Feb. 2022, pp. 152–177. DOI: 10.1177/87552930211042393

[22] A. P. Psathas, L. Iliadis, A. Papaleonidas, Strain Prediction of a Bridge Deploying Autoregressive Models with ARIMA and Machine Learning Algorithms, Commun. Comput. Inf. Sci., vol. 1826 CCIS, 2023, pp. 403–419. DOI: 10.1007/978-3-031-34204-2_34

[23] S. Singh, R. Shanker, Wireless sensor networks for bridge structural health monitoring: a novel approach, Asian J. Civ. Eng., vol. 24, no. 6, Sep. 2023, pp. 1425–1439. DOI: 10.1007/S42107-023-00578-5

[24] A. Mancini, G. Cosoli, A. Galdelli (+ another 6 authors), A monitoring platform for the built environment: towards the development of an early warning system in a seismic context, 2023 IEEE Int. Workshop on Metrology for Living Environment (MetroLivEnv), Milano, Italy, 29-31 May 2023, pp. 102-106. DOI: 10.1109/MetroLivEnv56897.2023.10164043

[25] S. J. Taylor, B. Letham, Forecasting at Scale, The American Statistician, vol. 72, 2018 - Issue 1: Special Issue on Data Science. DOI: 10.1080/00031305.2017.1380080

[26] Smart Data Models Program, Smart Data Models. Online [Accessed 23 August 2024] https://smartdatamodels.org/

[27] FIWARE Foundation, FIWARE - Open APIs for Open Minds. Online [Accessed 17 May 2022] https://www.fiware.org/

[28] A. Mobili, G. Cosoli, N. Giulietti (+ another 5 authors), Biochar and recycled carbon fibres as additions for low-resistive cement-based composites exposed to accelerated degradation, Constr. Build. Mater., vol. 376, May 2023, p. 131051. DOI: 10.1016/J.CONBUILDMAT.2023.131051

[29] J. Korstanje, Advanced forecasting with python: With state-of-the-art-models including LSTMs, Facebook's prophet, and Amazon's DeepAR, Adv. Forecast. with Python With State-of-the-Art-Models Incl. LSTMs, Facebook's Prophet. Amaz. Deep., July 2021, pp. 1–296. DOI: 10.1007/978-1-4842-7150-6

[30] F. Lamonaca, P. F. Sciammarella, C. Scuro, D. L. Carni, R. S. Olivito, Synchronization of IoT Layers for Structural Health Monitoring, Proc of the Workshop Metrol. Ind. 4.0 IoT, MetroInd 4.0 IoT, Brescia, Italy, 16-18 April 2018, pp. 89–94. DOI: 10.1109/METROI4.2018.8428329

[31] D. L. Carni, C. Scuro, F. Lamonaca, R. S. Olivito, D. Grimaldi, Damage analysis of concrete structures by means of B-value technique, Int. J. Comput. 16 (2017), pp. 82–88. DOI: 10.47839/ijc.16.2.884

[32] N. Shen, L. Chen, R. Chen, Multi-route fusion method of GNSS and accelerometer for structural health monitoring, J. Ind. Inf. Integr. 32 (2023), 100442. DOI: 10.1016/J.JII.2023.100442

[33] S. Hassani, U. Dackermann, M. Mousavi, J. Li, A systematic review of data fusion techniques for optimized structural health monitoring, Inf. Fusion. 103 (2024), 102136. DOI: 10.1016/J.INFFUS.2023.102136